IEEE Access
Multidisciplinary | Rapid Review | Open Access Journal

Received January 13, 2020, accepted January 26, 2020, date of publication February 7, 2020, date of current version February 18, 2020.

Digital Object Identifier 10.1109/ACCESS.2020.2972412

A Comparison of Power Conversion Systems for Modular Battery-Based Energy Storage Systems

FRANCISCO DÍAZ-GONZÁLEZ, DANIEL HEREDERO-PERIS, MARC PAGÈS-GIMÉNEZ, EDUARDO PRIETO-ARAUJO, (Member, IEEE), AND ANDREAS SUMPER, (Member, IEEE)

Centre d'Innovació Tecnològica en Convertidors Estàtics i Accionaments, Department of Electrical Engineering, ETS d'Enginyeria Industrial de Barcelona, Universitat Politècnica de Catalunya, 08028 Barcelona, Spain

Corresponding author: Francisco Díaz-González (francisco.diaz-gonzalez@upc.edu)

This work was supported in part by the European Union's Horizon 2020 Programme under Grant 773715, and in part by the Ministerio de Economia, Industria y Competitividad (Spanish Government) under Grant ENE2017-86493-R.

ABSTRACT A modular battery-based energy storage system is composed by several battery packs distributed among different modules or parts of a power conversion system (PCS). The design of such PCS can be diverse attending to different criteria such as reliability, efficiency, fault tolerance, compactness and flexibility. The present paper proposes a quantitative and qualitative comparison among the most widely proposed PCSs for modular battery-based energy storage systems in literature. The obtained results confirm the high performance of those PCSs based on the parallel connection of different modules to a single point of common coupling, also identifying those based on modular multilevel cascaded converters as promising concepts according to the assumptions of the present paper.

INDEX TERMS Hybrid energy storage systems, batteries, power electronics.

I. INTRODUCTION

Energy storage systems are progressively gaining momentum in diverse strategic fields such as the electromobility, renewable-based generation systems and power networks [1]. In this regard, special emphasis is in electrochemical technologies, i.e. batteries. One indicator of this is the fact that at the time of writing this article, 63% of about the 1623 projects listed in [2] are around electrochemical techonologies — an institutional database (Department of Energy of the United States) collecting projects involving the implementation of energy storage systems in different environments related to electric vehicles, renewables and power networks worldwide-.

An energy storage system is composed by three main parts: i) the energy storage containers, e.g. the batteries; ii) the power conversion system, e.g. the power electronics; and iii) ancillary balance of plant components, e.g. cooling, protections, monitoring subsystems and etcetera. Power conversion system (PCS) is as important as the storage container itself, since it permits a controlled, secure and efficient power exchange with the system the energy storage system is connected to. The topology of PCSs can be diverse depending on many factors, such as the size of the energy storage system, as well as on the requirements on efficiency, reliability, volume, modularity and so on. Precisely while facing a modular energy storage system, the industry and the academia have proposed so far several proposals and their study and comparison is the main object of the present paper.

Work in [5] suggests a qualitative comparison among different PCSs, resulting into a general approach to the knowledge field. It focuses on topologies for modular PCSs integrating either ac systems (e.g. a wind turbine or a flywheel), or dc systems (e.g. PV panels or batteries). For all cases, topologies are based on the interconnection of 1-phase or 3-phase H-bridges, operated as dc-dc or dc-ac converters. For instance, in the case of considering batteries, the reviewed topologies consider an H-bridge operated as a dc-dc converter, connected to the dc-link of a front-end dc-ac three phase H-bridge inverter, which interfaces with the external ac grid. This is, in fact, the most typical PCS applied on field. However, the paper does not address other promising topologies, such as those based on modular multilevel cascaded converters (MMCCs). Work in [4] complements that offered in [5] by analyzing the above mentioned MMCCs (a specific type: single star configuration), the above mentioned typical two conversion step PCS applied on field, and a third PCS. This third PCS comprises two conversion steps.

The associate editor coordinating the review of this manuscript and approving it for publication was Khmaies Ouahada.

The first conversion step is based on the cascade connection of dc-dc converters, each integrating a battery pack. The terminals of the cascade association of such converters is then connected to the dc-link of a front-end dc-ac converter, which interfaces with the external ac grid. Comparison among topologies is mainly focused on energy efficiency. To this end, various scenarios are proposed, all feeding loads at the low voltage grid. This work concludes that a MMCC installed at the medium voltage grid and the typical two conversion step PCS installed at the low voltage are comparable in terms of energy efficiency while accounting on distribution losses of the medium and low voltage grids from the MMCC to the load. Deeping further on topologies based on MMCCs, [3] offers detailed analysis on efficiency, operational flexibility and cost (evaluated from the size and number of components involved). In particular, the topologies addressed are a MMCC in single star configuration and a MMCC in double star configuration. This work concludes that the MMCC in single star configuration is superior over the double star one in terms of efficiency, cost (reduced number of components) and operational flexibility (battery handling). This conclusion is partly divergent with that achieved in [6], as selecting the MMCC in double star as the preferable option. As in [3], work in [6] concludes that the MMCC single star configuration is the one with lowest cost. However, [6] selects the MMCC double star as the best one in terms of efficiency. This divergence in criteria around energy efficiency can be explained due to the particular converter design assumptions for each of the studies. Work in [6] also concludes that the MMCC double star is the best option in terms of reliability and because of the possibility of applying this topology for future applications beyond that of a stand-alone battery-based system. This refers to the possibility of straightforwardly interconnecting the converter to an external dc network (e.g. LVDC, MVDC and HVDC applications). Similarly, [7] also analyses the MMCC single star configuration, with batteries splitted through each of the modules of the MMCC. The complementarity with previous works is in regard of the analysis of fault tolerance. Laboratory experiments confirm the excellent performance of such topology under 1-phase, 2-phase and 3-phase voltage sags with a depth of 100%. As for other previously mentioned works, from [7] the challenging control of the converter is highlighted as a main concern for MMCC topologies in general. Such control complexity is, in fact, higher than for the other topologies presented above.

Summarizing, previously presented works analyse in depth the operation and performance of specific topologies even including relevant technical comparison among some of them. However, such detailed analyses do not provide an overall view of the most representative PCSs for battery applications.

The present paper proposes a qualitative and quantitative comparison among different PCSs for modular energy storage systems. It contributes in covering at once the most widely proposed PCSs, according to a literature review. Further, the present paper addresses several aspects in regard of the comparison among PCSs, such as: reliability, efficiency, fault tolerance, compactness and flexibility. The latter aspect, among others, refers to the possibility of hybridizing the storage solution by including batteries of different characteristics. Altogether, the exercise carried out in this work aims to provide general criteria at the time of designing a modular battery-based solution. The assessment of the different comparison criteria is based on state-of-the-art techniques. With the aim of comparing the different PCSs in a fair way, common assumptions for all PCSs are adopted.

The contents of the paper are distributed as follows. Section 2 offers a first classification of PCSs based on an extended literature review. After such classification, section 3 addresses a comparison among the PCSs. This comparison is with respect to reliability, efficiency, fault tolerance, compactness and operational flexibility. To fairly compare PCSs, the main assumptions for analysis and adopted computation methods are also included in this section 3. The main results of section 3 are synthesized in section 4. Finally, section 5 emphasize in the main conclusions from the work.

II. CLASSIFICATION OF POWER CONVERSION SYSTEMS

This section firstly offers a classification of the most representative modular PCSs for battery-based systems. A graphical summary of the resultant catalogue is presented in Figure 1. The first three rows of Figure 1 present the general topologies for the PCSs. Please note that shaded boxes depicting dc-ac and dc-dc. These are the modules simply indicating at this point the type of voltage and current waveforms at their input and output terminals. The internal topology of modules can consider one or more power conversion steps yielding different module variants. Such variants at module level are included in the last row of Figure 1. This way, for instance, the three phase inverters shaded in grey for PCS #1, may include just conversion step, yielding variant #1a; two conversion steps, yielding variant #1b; or three conversion steps also incorporating galvanic isolation to the battery cells, yielding variant #1c. This definition of variants, or different topologies at module level, is adopted for the presentation of all PCSs in this article. In addition, boxes depicting capacitor and inductance symbols simply represent the location of passive components, regardless their type and design. Further, the light gray colouring the transformer included in each of the PCSs, indicates that the inclusion of this equipment at the point of common coupling with the external grid is optional. Following contents briefly describe each of the PCSs in Figure 1 along with their variants at module level.

One of the straightforward strategies to connect a modular battery-based system to the grid is configuring a PCS based on the idea of parallelizing inverters, each one holding part of the total number of battery cells in series/parallel configuration. For the purposes of the present paper, this would result in a PCS called number #1, which can be deployed in the variants #1a to #1c. The variant #1a, proposes the direct connection of a certain number of battery cells in the dc-link of the inverter of a module, or power train. As a difference, the #1b

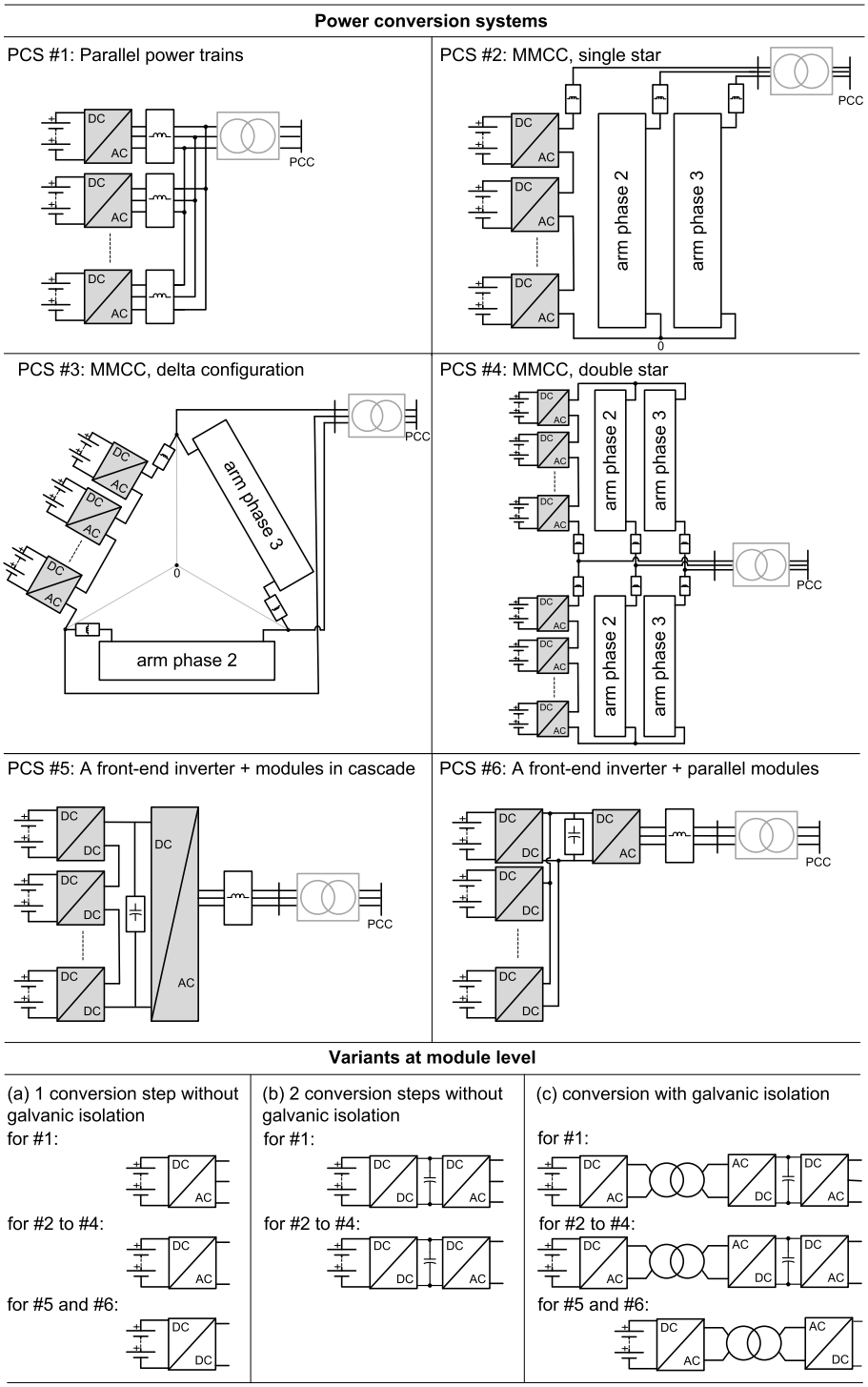

FIGURE 1. **Power conversion systems (PCSs) for modular battery-based energy storage systems.**

interfaces a dc-dc conversion step between the battery cells and the dc-link of the inverter. Further, the PCS number #1c provides this dc-dc conversion step with galvanic isolation.

The strategy #1 is highly reliable, since the failure of one power inverter does not disable the whole storage system. Other proposals in between the adoption of a non-modular PCS and fully modular PCSs as proposals #1a to #1c, have been already defined in literature. Contributing to the catalogue of PCSs for storage systems presented above, the PCSs number #2 to #4 are based on the adoption of modular multilevel cascade converters (MMCCs). The PCS number #2 corresponds to a MMCC, in which the modules are connected in

TABLE 1. Literature on PCSs for modular battery-based storage systems. Works reporting field experiences are marked in bold, and patents are noted in italics.

	Variants at module level			Applications	Main features
	(a) 1 conversion step (w/o galv. iso.)	(b) 2 conversion step (w/o galv. iso.)	(c) conversion with galvanic isolation		
#1: Parallel power trains	[11], [5]	[5], **[12]**, **[13]**, **[14]**, *[15]*	[16], [17]	EV motor drives, power network.	Low complexity, easy scalability.
#2: MMCC, single star	[18], [19], [20], [21], [22], [23], [24], [25][1], [26], [27], [28][1], [29][1]	[30], [31], [32][2]	[33]	EV motor drives, power network.	High voltage at the connection point, reduction of the size of coupling filters.
#3: MMCC, delta configuration	[34]	[32][2]	[31], [33]	Power network.	Even higher voltage at the connection point than with PCS #2 because of delta connection.
#4: MMCC, double star	[35], [36], [37], [38], [40], [41][2], [39][2] *[42]*	[6], [43], [44][2], [45][4]	[46], [47]	EV motor drives, power network, HVDC	Similar to PCS #2 but with extended power capacity.
#5: A front-end inverter + modules in cascade	[48][3,4], [49][3], [4], *[50]*[3], *[51]*	Does not apply	[52], [53], [54], *[55]*	Power network, EV charger	Fault tolerance.
#6: A front-end inverter + parallel modules	[56], [57], [58], [59], [60][2]	Does not apply	[57], [61], *[62]*	Power network, EV motor drives	High reliability and decoupling of the modules integrating batteries from the ac side.

[1] This work proposes a 1-phase converter.
[2] Dc-dc conversion step is based on half-bridge modules, and not H-bridge ones.
[3] This work concentrates on the dc-dc conversion step. The additional front-end inverter, as expected for PCSs #5, is not included since not required.
[4] This work does not concern the inclusion of batteries, but supercapacitors.

cascade so that they configure three arms. These arms share one common point configuring a single star. The topology for each of the modules may perform a single step dc-ac conversion without including galvanic isolation, yielding in this case the variant #2a. This one step conversion can be realized by an H-bridge cell (or bridge cell), or through a half-bridge cell (or chopper cell hereinafter). Analogously to the definition of variant #1b, variant #2b concerns a two step dc-ac conversion at module level, interfacing one dc-dc conversion phase. In turn, this dc-dc conversion phase, while provided with galvanic isolation, defines the variant #2c.

Similarly to what is suggested for PCS number #2, the structure of a PCS number #3 corresponds to a MMCC. However, the three arms of modules connected in cascade do not share any common point, but they are connected between them in delta configuration. Depending on the topology of each module, variants #3a to #3c are defined analogously to variants #1a to #1c (or #2a to #2c). This topology is typical for medium voltage Static Synchronous Compensators (STATCOM) [8].

Going further, one can extend the ratings of the PCS number #2 by doubling the number of arms building up the converter, so proposing 6 arms. In this configuration (named PCS number #4) each 3 arms share one common point thus configuring two stars (see Figure 1). Analogously to previous PCSs, variants #4a to #4c propose different topologies at module level. This topology is typical for high-voltage dc-transmission systems (HVDC) [9].

In the previously presented PCSs number #2 to #4, the ac terminals of a MMCC inverter are the front-end power electronic interfaces, from which the PCS can be coupled to an external grid (including a passive filter and/or galvanic isolation in between though). Conversely, the PCS number #5 also relies on a cascade association of H-bridge modules, but it serves not to perform a dc-ac transformation, but a dc-dc conversion instead. In this PCS number #5, the front-end dc terminals of the cascade association are connected to an inverter, which couples the system to the external grid. The dc-dc conversion step at each module of the cascade association can be provided with galvanic isolation or not, yielding variants #5c and #5a respectively. The variant #5b (2 power conversion steps at module level), does not apply for this PCS. Finally, while the modules in the PCS number #5 are connected in cascade, the PCS number #6 –along with variants #6a and #6c–, propose conversely the parallel connection of the modules.

To conclude, it is important to note that for PCSs number #1, #5 and #6, the topology of the front-end inverter can be realized in the form of the well known 2-level H-bridge structure, or as a multilevel neutral point clamped structure (NPC) [10], being the 3-level NPC structure the most approachable one.

Table 1 summarizes literature on the previously defined PCSs, covering both experiences in industry and academic research. Please note that literature works reporting field experiences are marked in bold, and patents are noted in italics. As it can be noted, the few field experiences reported in the table adopt PCS number #1, aiming to configure a highly redundant and reliable structure based on proven voltage source inverter technology. Alternatively, most of the

academic research go around the advance in MMCC-based structures. It is interesting to note also that the majority of cited literature concern one power conversion step modules. This way, the required galvanic isolation is in most of the cases shifted to the point of connection with the external network, as indicated in Figure 1.

The PCSs considered in this paper are identified as the most proposed ones in literature. However, such classification does not exclude the existence of other proposals. For the sake of completeness, some of them are listed in the following since considered particularly interesting:

- (Patent). A PCS composed by (from the connection point with the grid to battery packs) [63]: i) an ac-dc and dc-ac H-bridges in back-to-back configuration; ii) the parallel connection of high frequency transformers; iii) the inclusion of an ac-dc conversion step interfacing each of the transformer terminals and a battery pack.
- (Article). A PCS composed by (from the connection point with the 3-phase motor of an EV to battery packs) [64]: i) an ac-dc 3-phase inverter; ii) the cascade connection of dc-dc modules interfacing with different battery packs. The dc-dc modules include galvanic isolation, as for PCSs variant (c). So such description fits with PCS #5, however it is different in the sense that the cascade connection of dc-dc modules also includes a series capacitor and altogether yield the total voltage of the dc-link. The inclusion of such capacitor permits the dc-dc converters to exchange a power proportional to the difference between the total dc-link voltage and the batteries. At the end, this results into a smaller converter compared to PCS #5.

Following sections deep in the comparison among the various PCS topologies for modular battery-based solutions identified and classified in Figure 1.

III. COMPARISON AMONG POWER CONVERSION SYSTEMS

The previous section provides a first picture on PCSs for modular battery-based energy storage solutions. Deeping in the concepts presented in there, this section offers a comparison among different PCSs, focusing on various aspects such as reliability, efficiency, fault handling, compactness and flexibility. These aspects are addressed since being considered as principal for the design of PCSs. The latter aspect refers to the possibility of effectively configure hybrid energy storage solutions, by including different types of batteries. With the aim of conducting a fair comparison among PCSs, some assumptions are firstly stated, and these are presented in the following subsection:

A. ASSUMPTIONS

The following assumptions are adopted:

- The solution, as a whole, is rated at 30 kW and 60 kWh regardless the PCS topology. These power and energy storage capacities are distributed in 6 modules. Each module is composed by a battery pack and associated power conversion system rated at 5 kW / 10 kWh.
- The phase-to-phase voltage at the low voltage side of the coupling transformer of the PCSs with the external network is 400 V (phase-to-phase) for all cases.
- The rated voltage of each of the 6 battery packs configuring the system is 400 V. Packs are configured by standard 18650 type Lithium-ion cells [65]. A figure of merit for the capacity of each cell is usually around 2.5 Ah and the rated voltage is $V_{cell} = 3.7$ V, so to achieve 400 V at the pack terminals, 108 cells should be connected in series. Considering now the capacity of each string (2.5 Ah), to reach the required energy capacity of 10 kWh for the pack, 10 strings should be connected in parallel. The internal resistance of a cell, r_s, is in the range of milliohms (e.g. 55 mOhm) and the voltage at end-of-charge condition (fully charged) is $V_{cell_{eoc}} = 4.2$ V.
- The switching schemes for the different dc-dc and dc-ac converters building up the different PCSs are adopted from the state-of-the-art in this matter. A summary of the basis for each of them is presented in subsection III-A1. Detailed explanations are offered latter in the section.
- Given the voltage at the battery pack terminals, the voltage and the connection point of the PCS and the switching schemes, the voltages at the terminals of each of the modules composing the different PCSs are selected as the minimum recommended for a proper operation of the power electronics. This favors the performance of the PCSs. Further details on the calculation of voltage levels are offered in subsection III-A2.
- The transistor modules for each of the dc-dc and ac-dc converters of the different PCSs are differentiated with respect to the electrical magnitudes they should withstand. For 5 kW converters, the selected module is the model PS-22A78-E from Mitsubishi [66]. For low voltage ac-dc inverters of 30 kW (e.g. the front-end inverter in PCS #6), the selected module is the model QID3310006 from Mitsubishi [66]. The latter is also the module selected for medium voltage ac-dc inverters. The selection of the modules above is important for power losses calculation in Section III-C.

1) SWITCHING SCHEMES

The switching principles for H-bridge ac-dc, dc-dc as well as for MMCC structures are detailed in the following.

a: H-BRIDGE AC-DC CONVERTERS

H-bridge ac-dc converters are all operated under the two level Sinusoidal Pulse Width Modulation (SPWM) switching technique [67]. For one-phase H-bridge inverters, this is based on the application of two sinusoidal carrier signals, one per each of the arms of the converter, which are shifted π rad between each other. These two carriers are compared to a triangular high-frequency signal, and from these comparisons, the duty cycle for each of the two branches are deduced. Such operating mode permits to obtain, at the mid point of each

branch and with respect to the dc-link, three levels of voltage: 0 V, $-V_{bat}$, V_{bat}. The average voltage at the mid point of each of the branches a and b (so v_a and v_b) depends on the corresponding duty cycle D_1 and D_2, thus

$$v_a = V_{bat} \cdot D_1, \tag{1}$$
$$v_b = V_{bat} \cdot D_2. \tag{2}$$

Since the two sinusoidal carriers are complementary (they are shifted π rad), the duty cycles D_1 and D_2 are also complementary, thus

$$D_2 = 1 - D_1. \tag{3}$$

From above expressions, the instantaneous voltage at the AC terminals of the H-bridge can be calculated by,

$$v_{ab} = v_a - v_b = V_{bat} \cdot (1 - 2 \cdot D_2). \tag{4}$$

The voltage v_{ab} can also be renamed as v_z,

$$v_z = V_z \cdot \cos(\omega \cdot t + \phi), \tag{5}$$

being V_z the RMS value of the voltage waveform, ω the grid frequency and ϕ the grid angle. The term V_z is related to the dc-link voltage (i.e. the battery voltage) through the modulation index m as

$$m = \frac{V_z}{V_{bat}}, \tag{6}$$

so, v_z can be expressed as

$$v_z = V_{bat} \cdot m \cdot \cos(\omega \cdot t + \phi). \tag{7}$$

Matching now (4) and (5), the time dependent expressions for the duty cycles D_1 and D_2 can be expressed as

$$D_1 = \frac{1}{2} + \frac{1}{2} \cdot m \cdot \cos(\omega \cdot t + \phi), \tag{8}$$
$$D_2 = \frac{1}{2} - \frac{1}{2} \cdot m \cdot \cos(\omega \cdot t + \phi). \tag{9}$$

The expressions above serve to compute the conduction power losses at the transistors of the H-bridge, as presented later in section III-C. For calculating such losses, only the expression for D_1 is needed, as D_2 is complementary (see (9)).

At this point, it is also straightforward to obtain the duty cycle for the diodes in anti-parallel disposition in the H-bridge. The duty cycle is simply the complementary for D_1, so $D' = 1 - D_1$: diodes are driving current when transistors are not.

b: H-BRIDGE DC-DC CONVERTERS

For H-bridge operated as a dc-dc converter, the Unipolar Pulse Width Modulation (UPWM) technique is applied. It is based, as for the SPWM previously introduced, on the comparison of two carrier signals, one per converter arm, with a high frequency triangular waveform. Such comparison yields the triggering signals for transistors gate. The difference among the two techniques is that in UPWM the carriers are not sinusoidal waveforms but constant in time. As a consequence, not an ac voltage waveform is synthesized at the converter terminals but a dc waveform.

Addressing this, it is clear that the calculation of the duty cycles presented for the inverter case is not valid anymore. Duty cycle is constant in time now and depend on the magnitude of the dc voltage to be synthetized at the battery terminals with respect to the magnitude of the voltage at the dc-link and it varies between 0 and 1. Such voltage at the dc-link and the expression for duty cycle calculation is presented in the following, while addressing required voltage levels.

c: MMCC STRUCTURES

The switching of ac-dc the modules for MMCC structures is based on the two-level SPWM technique previously presented. The difference is that the duty cycles can be calculated using different type of carriers [68], [69]. For this article, a phase-shifted SPWM strategy is employed. It consists on using a carrier per module which is shifted depending on the available modules per arm. For instance, for a n module arm, the carrier per each module is shifted $2 \cdot \pi/n$ rad. As a result of such shifting, the voltage across the arm is shared among the modules.

2) VOLTAGE LEVELS

Table 2 summarizes the voltage levels at the different interfaces between components within each PCS. For instance, for PCS #1a, the description provided in the table indicates that the voltage ratings of the dc-ac converter interfacing the battery with the coupling transformer are 400 Vdc at the battery side, and 230 Vac at the transformer side. The description also indicates that each of the power trains composing the PCS is connected to the phase-neutral terminals of the transformer.

As noted in Table 2, given the rated voltage of 400 V for battery packs, the voltage level at the other side of dc-dc converters directly interfacing with batteries is set at 460 V. The calculation of such value is presented in the following section.

The voltage at the above mentioned point, and according to the assumptions in subsection III-A, should be set as the minimum required one for maximum performance. The minimum required dc-link voltage can be deduced from the case a unitary duty cycle is to be applied. Maximum duty cycle (D_{max}) is for the case the battery voltage is also maximum and it is still being charged at nominal current. Under these operating conditions, and considering the voltage drops at the inductive filter interfacing the converter and the battery, as well as those at the switches, the minimum required voltage at the dc-link of the converter can be calculated as

$$V_{dc} \geq \frac{I \cdot (2 \cdot r_{ce} + r_l + r_s \cdot n_s/n_p) + 2 \cdot V_{ce} + V_{bat_{eoc}}}{2 \cdot D_{max} - 1}, \tag{10}$$

being I the nominal current through the battery pack, calculated as $I = P_{bat}/V_{bat}$; r_{ce} the internal resistance of the transistors and V_{ce} the corresponding voltage drop; n_s and n_p the number of cells in series and in parallel configuring

TABLE 2. Voltage levels for each PCS.

PCS	Voltage levels (from battery pack to network connection)
#1a	Battery: 400 Vdc / dc-ac: 230 Vac (phase-neutral coupling transformer).
#1b	Battery: 400 Vdc / dc-dc: 460 Vdc / dc-ac: 230 Vac (phase-neutral coupling transformer).
#1c	Battery: 400 Vdc / dc-ac: 230 Vac / high frequency transformer ratio 1:1 / ac-dc: 400 Vdc / dc-ac: 230 Vac (phase-neutral coupling transformer).
#2a	Battery: 400 Vdc / dc-ac: 115 Vac / 2 converters in cascade yields 230 Vac per arm (phase-neutral of coupling transformer).
#2b	Battery: 400 Vdc / dc-dc: 460 Vdc / dc-ac: 115 Vac / 2 converters in cascade yields 230 Vac per arm (phase-neutral coupling transformer).
#2c	Battery: 400 Vdc / dc-ac: 230 Vac / high frequency transformer ratio 1:1 / ac-dc: 400 Vdc / dc-ac: 115 Vac / 2 converters in cascade yields 230 Vac per arm (phase-neutral of coupling transformer).
#3a	Battery: 400 Vdc / dc-ac: 200 Vac / 2 converters in cascade yields 400 Vac per arm (phase-phase coupling transformer).
#3b	Battery: 400 Vdc / dc-dc: 460 Vdc / dc-ac: 200 Vac / 2 cascaded converters yields 400 Vac per arm (phase-phase coupling transformer).
#3c	Battery: 400 Vdc / dc-ac: 230 Vac / dc-ac: 200 Vac / high frequency transformer ratio 1:1 / ac-dc: 400 Vdc / dc-ac: 200 Vac / 2 converters in cascade yields 400 Vac per arm (phase-phase coupling transformer).
#4a	Battery: 400 Vdc / dc-ac: 230 Vac (phase-neutral point of each star).
#4b	Battery: 400 Vdc / dc-dc: 460 Vdc / dc-ac: 230 (phase-neutral point of each star).
#4c	Battery: 400 Vdc / dc-ac: 230 Vac / high frequency transformer ratio 1:1 / ac-dc: 400 Vdc / dc-ac: 230 Vac (phase-neutral point of each star).
#5a	Battery: 400 Vdc / dc-dc: 460 Vdc / 6 converters in cascade yields 2760 Vdc / 3-phase dc-ac: 400 Vac (phase-phase coupling transformer).
#5c	Battery: 400 Vdc / dc-ac: 230 Vac / high frequency transformer ratio 1:1 / ac-dc: 400 Vdc / 6 cascaded converters yields 2400 Vdc / 3-phase dc-ac: 400 Vac (phase-phase coupling transformer).
#6a	Battery: 400 Vdc / dc-dc: 800 Vdc / 3-phase dc-ac: 400 Vac (phase-phase coupling transformer).
#6c	Battery: 400 Vdc / dc-ac: 230 Vac / high frequency transformer ratio 1:1 / ac-dc: 800 Vdc / 3-phase dc-ac: 400 Vac (phase-phase coupling transformer).

the battery pack; r_s the internal resistance of battery cells; and $V_{bat_{eoc}}$ the voltage of a battery cell at the end-of-charge condition, which can be calculated by the product of $V_{cell_{eoc}}$ and n_s.

Once the minimum required dc-link voltage is calculated, the duty cycle to be applied by the converter while charging the battery at nominal operating conditions (both in current and voltage for the battery pack), can be easily computed by

$$D = \frac{1}{2}\left(1 + \frac{I \cdot (2 \cdot r_{ce} + r_l + r_s \cdot n_s/n_p) + 2 \cdot V_{ce} + V_{bat}}{V_{dc}}\right) \quad (11)$$

Finally, just include some notes on the voltages presented in the table around the ac voltage synthetized by the inverters directly interfacing with battery packs. Such voltage is 230 Vac, which means that the modulation factor to be applied by the inverter is $m = 230 \cdot \sqrt{2}/400 = 0.810$. This modulation factor ensures a safety operating point for the inverter while it is high enough to ensure the proper utilization of inverter capabilities.

B. DISCUSSION ON RELIABILITY

The term reliability refers to the ability of a system or component to perform its required functions under stated conditions for a specified period of time [70]. A way to estimate the reliability of a system is calculating the so-called mean-time between failures (MTBF). This metric is typically expressed in hours. In general terms, the higher the MTBF, the higher the reliability of a product is.

Using the parts count prediction method, included in the MIL-HDBK 217, the failure rate for a component or system λ (usually expressed in failures / 10^6 hours) can be computed by

$$\lambda = \sum_{i=1}^{n} N_i \cdot (\lambda_g \cdot \pi_Q)_i, \quad (12)$$

where λ_g is the generic failure rate for the i^{th} generic part, expressed in [failures / 10^6 hours]; π_Q is the corresponding quality factor; N_i is the quantity of the i^{th} generic part; and n is the number of different parts in the component or system being evaluated.

For electronic systems, in which unlike mechanical ones there are not moving parts, it is generally accepted a constant failure rates during the useful operating life. Doing this, the predicted reliability for a component or system at specific operating life in hours $R(t)$, can be computed by

$$R(t) = e^{-\lambda \cdot t}, \quad (13)$$

and is expressed in per unit adopting values between 0 and 1. As noted, reliability function presents an exponential shape.

Method MIL-HDBK-217F offers a data base for electronic components [71]. Assuming quality factor $\pi_Q = 1$ in all cases, the typical failure rate λ for the main components building up the different PCSs to be evaluated are: $\lambda_{Mosfet} = 1.1 \cdot 10^{-9}$ failures / hour for MOSFETs; $\lambda_{Diode} = 7.5 \cdot 10^{-9}$ failures / hour for diodes; $\lambda_{Inductor} = 2.0 \cdot 10^{-10}$ failures / hour for an inductor; $\lambda_{Capac} = 2.5 \cdot 10^{-9}$ failures / hour for a capacitor; $\lambda_{LF-tr} = 3.6 \cdot 10^{-7}$ failures / hour for a low frequency transformer; $\lambda_{HF-tr} = 9.6 \cdot 10^{-7}$ failures / hour for a high frequency transformer. From the failure rate of individual components and using equation (12), the failure rate for the ac-dc and dc-dc H-bridge, as well as for 3 phase H-bridge inverter results: $\lambda_{bridge} = 3.4 \cdot 10^{-8}$ failures / hour for the ac-dc and dc-dc H-bridge; and $\lambda_{3-bridge} = 5.2 \cdot 10^{-8}$ failures / hour for the 3 phase bridge. Finally, the typical failure rate for a battery pack is assumed as $\lambda_{bat} = 1.0 \cdot 10^{-5}$ failures / hour. For the purposes of the present paper the battery ageing is not considered and thus the parameter λ_{bat} is let as constant. Similarly, the failure rates for semiconductors are also considered as constant, regardless the particular current and voltage stress. This enables the direct application of method MIL-HDBK-217F adopting published data in the corresponding data base.

Now, applying equation (13), and for a lifespan of 50,000 hours, which is a usual number for reliability

TABLE 3. Reliability for each of the components configuring the PCSs.

Component	Symbol	Value
MOSFET	R_{Mosfet}	0.999945
Diode	R_{Diode}	0.999625
Inductor	$R_{Inductor}$	0.999990
Capacitor	R_{Capac}	0.999875
Low-frequency transformer	R_{LF-tr}	0.982161
High-frequency transformer	R_{HF-tr}	0.953133
1-phase H-bridge	R_{bridge}	0.998281
3-phase H-bridge	$R_{3-bridge}$	0.997423
Battery	R_{bat}	0.606530

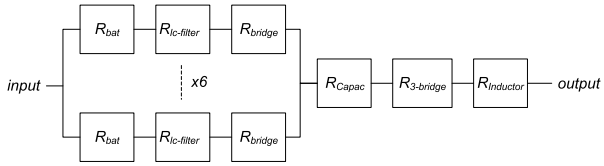

FIGURE 2. Reliability block diagram for PCS #6 variant (a).

TABLE 4. Estimation of reliability for the PCSs.

	Variants at module level		
	(a) 1 conv. step	(b) 2 conv. step	(c) with galv. iso.
#1	0.996225	0.996160	0.994105
#2	0.745779	0.744150	0.700043
#3	0.745779	0.744150	0.700043
#4	0.996225	0.996160	0.994105
#5	0.049103	-	0.036437
#6	0.993524	-	0.991498

calculations, the reliability for each of the above components is summarized in Table 3.

Once the reliability of each individual component is calculated, one can calculate the reliability of each of the proposed PCS. To do so, the reliability block diagram method is adopted [72]. This method permits to estimate the reliability of a system in which blocks (or components) are connected in series and/or parallel. For block connected in series, the associated reliability becomes

$$R_{series} = \prod_{i=1}^{n} R_i, \tag{14}$$

while for blocks in parallel, it becomes

$$R_{parallel} = 1 - \prod_{i=1}^{n} (1 - R_i). \tag{15}$$

Applying the algebra above, the reliability of each of the proposed PCSs can be calculated. Results are presented in Table 4. As an example, the reliability block diagram for PCS #6 is presented in Figure 2. The block diagrams for the rest of the PCSs (variant a)) are included in the Appendix.

From Figure 2, the mathematical function for reliability calculation of PCS #6 variant (a) is

$$R_{PCS6a} = R_{ind} \cdot R_{3-bridge} \cdot R_{cap} \cdot (1 - (1 - R_{bat} \cdot R_{lc-filter} \cdot R_{bridge})^6). \tag{16}$$

From the results in Table 4, it can be observed that PCS #1, in all proposed variants, is intended as the most reliable one. This might be, in fact, one of the reasons because this topology has been actually built and installed in field (apart from others such as previous expertise of industry in developing the technology included in there). By parallelizing diverse power trains, the failure in one of them does not necessarily provoke the interruption of the whole system. Under such circumstance, the ac terminals of the power train affected by the eventuality could be easily disconnected from the rest of the system through a conventional low voltage breaker.

With the same expected reliability of PCS #1 we have the PCS #4 (an MMCC double star topology). Given 6 battery packs, the double-star concerns just one block per each arm. At the end, the double star configures six blocks connected in parallel, so with the same reliability of PCS #1. However, the way of managing the PCS #4 is more complicated than for PCS #1 in case of an eventuality in one of the battery modules. For instance, if one of the converter arms fails, the entire phase unit operation is disabled. The PCS could still be operated under bipolar mode though.

Anyhow, despite the challenging management of MMCCs, and also in regard of a comparison of reliability for PCS #1 and #4, [40] concludes that the reliability of the latter is even higher than for the PCS #1 till reaching loading rates up to 93% with respect to the ratings of the particular system considered in this work. The reason supporting this conclusion is that for very high loading rates, all modules of the MMCC should work (there are no modules in idle mode anymore) so a failure of one of them can be critical, thus sensibly lowering the reliability of the whole system.

Immediately below PCS #1 and #4 in reliability, we find PCS #6. Either in variant (a) or (c), the connection of battery modules in parallel yields a very high reliability. The little difference with PCS #1 (the topology with maximum reliability) is because of the fact that an eventuality in the 3-phase grid side inverter would disable the whole PCS.

Further, with a sensibly lower reliability than for PCS #1, we find PCSs #2 and #3. These topologies (MMCC in star and delta configurations) offer interesting features. Given 6 battery packs, these are distributed in pairs, one pair per arm, which is then directly connected to the grid connection point. At the end, in both star and delta configurations, three strings of batteries (i.e. two battery packs in series) are seen in parallel configuration from the point of view of the network, so an eventuality in one battery pack would disable one arm (i.e. two battery packs), letting the other two ones still available, so 67% of the rated power still in operation.

Finally, PCS #5 present the lowest reliability among eligible. The connection of all battery packs in series and the need of interacting with the main grid through a single 3-phase inverter, make this topology as barely reliable. The obtained value for reliability (e.g. 0.049103 for variant (a)) means that the probability of experiencing a failure disabling the whole PCS during the 50,000 hours of expected lifespan is very high.

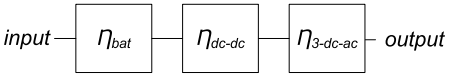

FIGURE 3. Efficiency block diagram for PCSs #6 and #5 variant (a).

C. DISCUSSION ON EFFICIENCY

Assessing the efficiency of each of the PCSs under discussion is a challenging task. The efficiency depends on the number of power converters included in each PCS, their voltage and current ratings, and the way they are connected between each other and operated (switching techniques). The aim of the following lines is just to provide rough estimations making the comparisons as fair as possible. To do so, the assumptions presented at the beginning of section III are adopted. An additional assumption is that for efficiency calculations, the following losses are to be considered: i) those in the transistors (both conduction and switching ones) configuring the H-bridge converters or modules building up the PCSs; ii) those associated to battery packs; iii) and those associated to high-frequency transformers. Thus, losses in passive components are not addressed, since these are not –but the losses in the transistors– what mostly determine the efficiency of the modules.

The first step to assess the efficiency is to present a common methodology. Similar to the assessment of reliability in section III-B, the efficiency of each PCS is based on mathematical expressions built up from the particular efficiency of each module, all configuring efficiency block diagrams. So, for instance, the efficiency block diagram for PCS #6 (variant (a)), is plotted in Figure 3. This block diagram also applies for PCS #5 variant (a).

As can be noted, the efficiency of the whole PCS #6 variant (a) can be simply resembled to the efficiency of one of the 6 power trains comprised by the series connection of a battery pack and a dc-dc conversion step, all connected to the front-end dc-ac converter. Such efficiency is calculated by the product of the particular efficiency of the different elements connected the way described above, so

$$\eta_{PCS6a} = \eta_{bat} \cdot \eta_{dc-dc} \cdot \eta_{3-dc-ac}, \tag{17}$$

being η_{PCS6a} the efficiency of the whole PCS, η_{bat} the efficiency of a battery pack, η_{dc-dc} the efficiency of the H-bridge working as a dc-dc converter, and $\eta_{3-dc-ac}$ the efficiency for a three-phase H-bridge inverter.

For the sake of completeness, the block diagrams for the rest of PCSs considered in this paper (variant (a)), as well as the corresponding mathematical expressions for efficiency calculations, are presented in the Appendix.

As previously introduced, the accuracy for the estimation of the efficiency of the different PCSs relies on the estimations for the efficiency of particular components (batteries, H-bridges and so on) and these depend on the operating conditions (see subsection III-A).

The power converters building up the different PCSs are all based on H-bridges, either one-phase or three-phase ones, operated under SPWM or UPWM switching schemes. Following contents describe the formulas for switching and conduction power losses calculation of the transistors (and corresponding diodes in anti-parallel disposition) under above mentioned switching schemes [73].

1) H-BRIDGE AC-DC CONVERTER

Once the duty cycle D is known, the conduction power losses for a transistor can be calculated by

$$P_{tr-c} = \frac{2}{\pi} \int_0^{\pi/2} (v_{ce} \cdot i \cdot D) \cdot d\theta, \tag{18}$$

being i the current actually exchanged with the grid and v_{ce} the collector emitter voltage drop at the transistor. The current i can be expressed as

$$i = \sqrt{2} \cdot I \cdot \cos(\theta). \tag{19}$$

The voltage v_{ce} can be shaped to a curve depending on the current i in the form of

$$v_{ce} = U_0 + r \cdot i^b, \tag{20}$$

being U_0, r and b shaping parameters deduced from the datasheet provided by transistors' manufacturer.

The calculation of the conduction power losses for a diode P_{di-c} can be calculated analogously, just replacing D by D' and the new expression for v_{ce} considering the diode characteristics.

The switching power losses for a transistor does not depend on the duty cycle but on the switching frequency along with the energy lost in one turn-on and turn-off event during a period. These energies can be associated to from mathematical functions shaping the curves provided by manufacturers in their datasheets. These curves are depending on the driving current I (RMS value) through the transistor. For the energy lost while turning on, for instance, this function can have the form of

$$E'_{on} = \frac{I^k}{\beta}, \tag{21}$$

being k and β the shaping parameters. The curves provided by manufacturers are usually expressed considering standard dc-voltage voltage across the transistor, named as V_{cc}. In the present case this is V_{bat}, so E'_{on} can be corrected by

$$E_{on} = E'_{on} \cdot \frac{V_{bat}}{V_{cc}}. \tag{22}$$

Using now the expression for E_{on} (and that analogously proposed for E_{off}), the power losses for a transistor for a switching period is

$$P_{tr-sw} = \frac{1}{\pi} \int_0^{\pi/2} (E_{on} + E_{off}) \cdot f_c \cdot d\theta, \tag{23}$$

being f_c the switching frequency in Hertz.

The switching power losses for a diode can be calculated adopting an analogous procedure than for transistors. Here,

manufacturers are providing information for the turn-off process, because it is when losses are incurred. For that situation, energy lost is named as E_{rr} and the expression for power losses calculation is

$$P_{di-sw} = \frac{1}{\pi}\int_0^{\pi/2} E_{rr} \cdot f_c \cdot d\theta. \quad (24)$$

From above expressions, the total power losses for a H-bridge operated as an inverter are given by

$$P_{ac-dc} = 4 \cdot (P_{tr-sw} + P_{di-sw}) + 4 \cdot (P_{tr-c} + P_{di-c}). \quad (25)$$

In turn, the efficiency is expressed as

$$\eta_{ac-dc} = 1 - \frac{P_{ac-dc}}{P_{bat}}, \quad (26)$$

being P_{bat} the power provided by the battery pack.

2) H-BRIDGE DC-DC CONVERTER

The expressions for power losses calculation previously introduced can be essentially used for a H-bridge operated as a dc-dc converter under the UPWM switching technique. Some changes should be applied though and these are introduced in the following.

Given the duty cycle D and current i as calculated above, the expressions (18) and (23) for power losses in transistors can be directly adopted. In dc-dc operating mode, diodes are never driving so there are no losses incurred in them and total power losses in the converter are given by

$$P_{dc-dc} = 4 \cdot (P_{tr-sw} + P_{di-sw}). \quad (27)$$

Once the methodology for efficiency calculation has been presented, following contents address the efficiency comparison among PCSs. Previously though, some required notes introduced around the efficiency of the battery packs and the high frequency transformer. The efficiency of these components is considered constant for all PCSs since the operating conditions are the same for all cases. The efficiency for both low and high frequency transformers is very high. For low frequency transformers, it typically reaches –and even exceeds– 99% for medium-sized (tens of kVA) transformers. The efficiency of high-frequency ones could result increased because core losses are function of frequency (see Steinmetz equation [74]). On the other hand though, the core materials utilized in high frequency transformers have an hysteresis cycle much more narrow than that for the materials in low frequency transformers. At the end, the efficiency of high frequency transformers can result as high as for low frequency ones. As a figure of merit, in this work an efficiency of 99% is also assumed for this type of transformers. In regard of battery packs, an efficiency around 97% is assumed.

Finally, adopting the efficiency block diagrams along with the methodology and assumptions for efficiency estimation of the different components, the efficiency of the different PCSs proposed in this paper are summarized in Table 5.

Table 5 clearly shows that the efficiency reduces along with the complexity of the PCSs. This is obvious while comparing, for instance, PCS #1 variant (a) with variants (b) and (c): the higher the number of components building up each of the power trains of the PCS is, the lower the expected efficiency.

TABLE 5. Comparison on energy efficiency for the proposed power conversion systems.

	Variants at module level		
	(a) 1 conv. step	(b) 2 conv. step	(c) with galv. iso.
#1	0.935	0.910	0.860
#2	0.902	0.876	0.830
#3	0.931	0.909	0.856
#4	0.935	0.910	0.860
#5	0.898	-	0.850
#6	0.923	-	0.867

Now comparing the efficiency among PCSs (just variants (a) and (b)), it can be deduced that the PCSs with the highest efficiency are the number #1 and #4. For variant (a), efficiency reaches the value of 0.935 p.u., while it is expected at 0.910 for variant (b). The parallel connection of power trains with the network coupling point in these topologies results into maximum efficiency. This might be one of the reasons supporting the wide implementation of PCS #1 by industry. According to the assumptions of the present work, PCS #4 results as efficient as PCS #1. However, this is because of the reduced number of modules composing the PCS. For large number of modules, in which some are connected in cascade in each of the arms of the PCS, the efficiency is expected to be lower than for PCS #1.

Anyhow, after PCSs #1 and #4, PCS #6 is identified as the most interesting one in terms of efficiency. For variant (a), the efficiency (0.923 p.u.) is quite similar to the efficiency for PCS #1. For variant (c), PCS #6 is even the best one among eligible. The parallel connection of dc-dc conversion steps to a common dc-link is thus identified as a promising option in terms of efficiency.

Then, with an efficiency of about 0.931 and 0.902 p.u. (variant (a)) we find PCSs #3 and #4 respectively. These PCSs are based on MMC topologies. The factor $\sqrt{3}$ affecting the current through the different modules in star configuration (PCS #3); and the voltage across the modules in delta configuration (PCS #4) respectively, yield an slightly lower efficiency for these PCSs in comparison to PCS #1.

Finally, with the poorest efficiency among eligible, we find PCS #5. Definitely, the configuration of dc-dc conversion steps in cascade is not convenient in terms of efficiency. The resultant dc voltage between the terminals of the cascaded association is high, yielding remarkable losses at the front-end inverter of the PCS.

D. DISCUSSION ON FAULT TOLERANCE

Several causes located at different locations can cause critical faults on some part of the electric conversion. Thus, the relevant parts to focus on fault tolerance topic are the converter itself (internal faults), and the cables (dc or ac).

On one hand, internal faults involve possible semiconductor faults such as short-circuit due to a bad behaviour of a

switch or an incorrect trigger signal. This situation is usually saved by specific hardware depending on the applied technology. Different solutions aims to protect the system permitting to block the semiconductor in a safe way. An example is to add a soft turn-off circuitry to the driver that manages the semiconductors. Thus, soft turn-off can be used for decreasing the turn-off voltage overshoots over the semiconductor switch when high currents are involved, avoiding a damage to the converter.

On the other hand, many authors are recently addressing the fault analysis hot topic applied to dc network cables and their dynamic effect [75]. As cited in [76], conventional converters (voltage source converters and MMCCs) are not able to isolate dc faults by themselves. These converters are vulnerable to dc-cable short-circuit and ground faults due to the high discharge current from the dc-link capacitance [77], being the most sensitive situation the pole-to-pole fault [76]. In fact, as detailed in [76], in some topologies like PCS #4, fault currents at the dc side, ac wires and in the converter exist all time, even after blocking the sub-modules of an arm phase. This is due to the behaviour as an uncontrolled rectifier. All these situations suppose that the fault located at the dc cabling should be isolated by additional devices. Some of the used alternatives are fast cutting-edge dc breakers [78], [79], modified ac breakers combined with fast static switches [80] or by means of modified converter sub-module units [81].

However, in the case of PCSs for modular battery-based energy storage systems a dc fault can be assumed as rare due the proximity between the storage system and the converter itself. In this sense, for the study case, the fault tolerance analysis is concentrated on the ac side fault. Some other authors, as [82], also attends to this kind of faults instead of dc ones. Actually, a wall bushing insulation fault is proposed by [82] as a probable source of ac faults. In that sense, and according to the different PCS topologies presented in Figure 1, a three-phase minimal conversion unit is hereinafter adopted for comparison of fault tolerance. Figure 4 depicts those minimal units connected to the utility per each PCS case. Conforming to this, PCS #1 will be the minimal unit reference. For the reference PCS (i.e. PCS #1), each connected battery pack voltage is V_{bat}, the PCS exchanges a power of S, can synthesize a phase-to-phase ac voltage of V_z, and is interfaced with the grid by means of an inductive filter, for simplicity.

Following this criteria, Table 6 shows seven values of comparison; maximum phase-to-phase ac side synthesizable voltage V_g, exchanged power P, rated ac filter current I_r, employed modulation technique, effective switching frequency and voltage drop that the inductive filter has at its terminals (ΔU & f_e) and, finally, the self-inductance value L. It should be noted that the modulation technique has been selected according to two possible situations. If the dc-ac involves a three-phase inverter it is assumed SPWM (case of PCS #1, #5 and #6). If the dc-ac involves an arm-phase submodule of a MMCC it assumed UPWM for optimal design

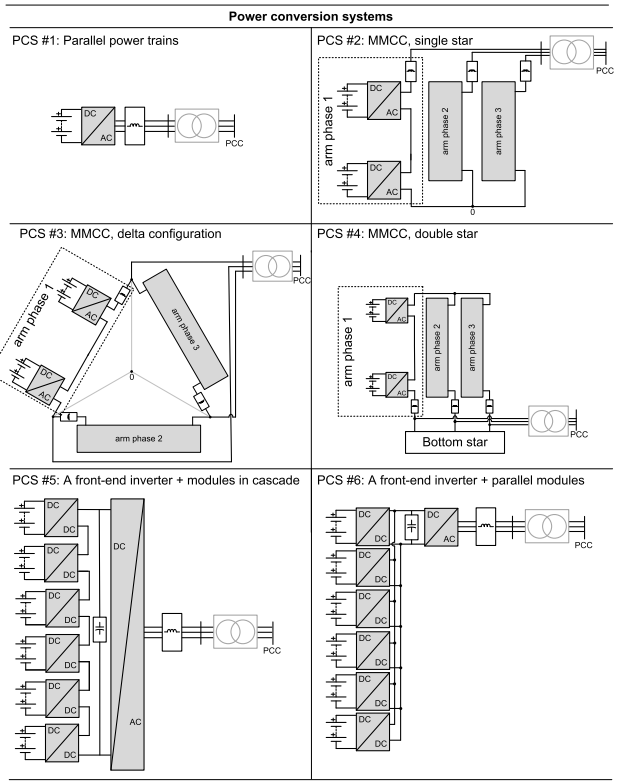

FIGURE 4. PCSs for modular battery-based energy storage systems highlighting in blue the minimal three-phase power unit connected to grid.

TABLE 6. Fault tolerance comparison according to minimal connected unit per each PCS topology.

Id.	V_g	P	I_r	Mod.	ΔU	f_e	L
PCS #1	V_z	S	I	SPWM	V_{bat}	f	L
PCS #2	$4V_z$	6S	$\frac{3}{2}$I	UPWM	$V_{bat}/2$	2f	$\frac{1}{6}$L
PCS #3	$\frac{4}{\sqrt{3}}V_z$	6S	$\frac{3}{2\sqrt{3}}$I	UPWM	$V_{bat}/2$	2f	$\frac{1}{4\sqrt{3}}$L
PCS #4[1]	$2V_z$	3S	$\frac{3}{2}$I	UPWM	$V_{bat}/2$	2f	$\frac{1}{3}$L
PCS #5[2]	$12V_z$	6S	$\frac{1}{2}$I	SPWM	$12V_{bat}$	f	24L
PCS #6[2]	$2V_z$	6S	3I	SPWM	$2V_{bat}$	f	$\frac{2}{3}$L

[1] The self-inductance is assumed to be splitted between top and bottom arms of each phase.

in terms of output current ripple (case of PCS #2, #3 and #4). Also, in case of dc-dc power stages involved, a 1:2 voltage ratio is assumed (case of PCS #5 and #4). Finally, each full PCS by a total of six conversion systems.

Once the values of Table 6 are obtained a common value for all PCS can be computed as an index to evaluate a PCSs fault tolerance. The adopted index is calculated as the ratio di/dt over I_r when a fault in the grid terminals appears, and the value of di/dt is computed as V_g/L from Table 6. This index is named FTI (Fault Tolerance Index).

The computation of the FTI for the different PCS minimal ac units can be seen in Table 7, assuming FTI in PCS #1 as the reference and equal to 1. The higher the FTI the lower the fault tolerance. In general terms, it can be deduced that MMCC are less fault tolerant to an AC fault.

TABLE 7. Fault Tolerance Index (FTI).

	FTI
PCS #1	1
PCS #2	16
PCS #3	$8/\sqrt{3}$
PCS #4	4
PCS #5	1
PCS #6	1

E. DISCUSSION ON COMPACTNESS

A straightforward method to assess compactness could be through components counting. To make this counting as fair as possible, a weighted sum is proposed, and weighted coefficients are depending on the power density, which are multiplied by the rated power of each of the components' type. The total volume for a PCS i, V_i, are calculated by

$$V_i = \sum_{j=1}^{J} n_j \cdot P_j \cdot \alpha_j^{-1}, \qquad \forall i \in I, \tag{28}$$

being I the set of PCSs to evaluate; J is the number of components' type in each of the PCSs; n_j is the number of times each of the components' type appears in each of the PCSs; P_j the rated power of the component; and α_j the weighted coefficient for each of the components' type.

The weighting coefficients (the power densities, in fact) are considered as typical values from commercial systems and the experience of the authors of the present paper. These are presented in the following:

- α_{LF-tr} for a low frequency transformer. This is assumed as 68 kVA/m^3. This is a typical power density for a three phase 30 kVA / 50 Hz transformer by one of the principal manufacturers [83].
- α_{HF-tr} for a high frequency transformer. This is assumed as 7395 kVA/m^3. This is derived from the characteristics of a commercial single phase transformer of 4 kVA approximately, working at frequencies in the range of tens of kHz and at voltages around 150 Vac [84].
- α_{mod} for an ac-dc or dc-dc module based on H-bridges. This is assumed as 215 kVA/m^3. This is derived from the characteristics of a commercial transformerless ac-dc inverter rated at 30 kW / 480 Vac [85].
- α_{bat} for a battery pack. This is assumed as 362 kWh/m^3, being obtained as detailed in the following. Firstly, note that the pack is based on 10 strings of 108 lithium-ion cells in series each. So, addressing the dimensions of a 18650 lithium ion cell (18 mm diameter times 65 mm height), and oversizing the pack 10% in volume for battery management system and ancillaries, the volume of a 10 kWh pack is estimated as 0.027 m^3. From this value the energy density indicated above can be easily calculated.

Applying the above formula and parameters to all considered PCSs, volumes can be calculated. The adopted assumptions for calculation are the same as for the rest of the paper, i.e. each battery pack is rated at 4.8 kWh; each corresponding power conversion module is rated at 5 kVA; and for PCS #5 and #6 the front end inverter is rated at 30 kVA. Results are presented in Table 8. Three main aspects are listed in the following.

TABLE 8. Estimation of volume for the PCSs.

	Variants at module level		
	(a) 1 conv. step	(b) 2 conv. step	(c) with galv. iso.
#1	0.740	0.878	1.020
#2	0.740	0.878	1.020
#3	0.740	0.878	1.020
#4	0.740	0.878	1.020
#5	0.878	-	1.020
#6	0.878	-	1.020

The estimated volume for variant (a) for PCSs #1 to #4 are equal, as well as that for variant (b) and (c). For variant (a), estimated volume is 0.740 m^3; 0.878 m^3 for variant (b); and 1.020 m^3 for variant (c). So the differences are not among PCSs, but among variants. This is because the above PCSs have the same number of battery packs, power modules and transformers (e.g. PCS #1 variant (a) has 6 power modules, 6 battery packs and 1 low frequency transformer, and this is also for PCS #2 variant (a)). So for PCSs #1 to #4, adopting the most complex variant (variant (c)), is translated into an increment in expected volume of nearly 40% with respect to the volume of the simplest variant (variant (a)).

Similarly, the estimated volume for variant (a) for PCSs #5 and #6 are equal, as well as that for variant (c). For variant (a), estimated volume is 0.878 m^3, while it is 1.020 m^3 for variant (c). So for these PCSs, adopting the most complex variant (variant (c)), is translated into an increment in expected volume of about 17% with respect to variant (a).

To sum up, and addressing now all PCSs at once, it is worth noting that any of them are assumed as impractical for excessive volume in comparison to the rest of the alternatives. Also, it is worth noting a non excessive increment (40% at most) while adopting the most complex variant with respect to variant (a).

F. DISCUSSION ON FLEXIBILITY

This section proposes a discussion on the flexibility of the PCSs. The term flexibility is intended here as the ability to manage a PCS in different operational circumstances such as the connection of batteries of different type in the diverse modules of the PCS. The inclusion of batteries with different voltage levels and characteristics (state-of-charge, admissible current rates, cyclability, and etcetera) challenges the operation and stability of the PCSs and this is topology dependent. Another circumstance can be the connection of the PCS to a weak grid, so the focus should be on power quality issues. Further even, another circumstance can be the need of balancing the state-of-charge of the different batteries connected in the diverse modules of the PCS. Altogether yields the flexibility as an important feature for a modular PCS, and this is briefly addressed in the following lines.

In general terms, and among considered options, the PCS #1, is the most flexible one. A proof of the high flexibility of

this topology is the fact that this option is recurrently adopted by the industry, as noted in Table 1. The parallel connection of different power trains to a common point with the external grid maximizes its flexibility. The batteries connected at the different power trains can be of diverse voltage, energy and power ratings, since the interaction between the power trains is minimum and these can be managed almost independently. One drawback of this PCS in regard of flexibility is that because of its high cost –each power train comprises a dedicated front-end inverter–, designers may consider the reduction of the number of power trains thus configuring large battery packs to fulfill the energy storage requirements. The variations of the voltage and internal impedance of battery packs with large number of cells in series and in parallel can affect the stability of the PCS in connection with the external grid, as addressed in [86], [87].

The flexibility for PCSs #2 and PCS #3 propose the connection different modules in cascade, and this poses challenges from an operational point of view. Such challenges are addressed in [31], where the operation of the converter under unbalanced grid conditions. Firstly, the work concludes that the operation of such PCSs under grid unbalances could be more challenging that for conventional three-phase topologies (e.g. PCS #1), since each of the PCS branch (either in star or delta configuration) is affected in different manner and thus, has to be operated differently. To facilitate this operation, the work also concludes that it is very convenient to opt for two conversion steps at module level (i.e. adoption of variant (b)). The second conversion step (i.e. the dc-dc converter interfacing with the battery terminals), avoids the transfer of harmonic currents experienced by the dc-link capacitor of the dc-ac H-bridge converter of the module. This is particularly important in the case of star connection (PCS #2). Under this configuration, the three arms of the PCS should generate the three-phase system sinusoidal voltage and current. This directly yields power fluctuations in the arms of double the grid frequency, so second order current harmonics flow through the dc-link capacitors of dc-ac modules in variant (a). These would be directly experienced by batteries without the inclusion of a second dc-dc conversion step [3], so such second conversion step is beneficial for the battery packs in regard of an extended lifetime. The second benefit from opting for variant (b) is related to the enhanced controllability of the state-of-charge of the different battery pack splitted throughout the PCS, as also addressed in [32].

The flexibility of PCS #2 is further investigated in [24], now considering batteries of different voltage at each of the modules of the PCS. The work highlights the possibility of doing so with this topology –not addressing though the difficulties identified above and derived from connecting in cascade different modules–. The work indicates the possibility of reducing the number of modules while considering some of them with increased battery voltages, and also of applying different switching techniques –advanced ones– at each module (e.g. high-frequency PWM for one cell and low-frequency switching rates at the others, as proposed in [88].)

Finally, also in regard of PCSs #2 and #3, just note that flexibility for variant (c) could be affected by the relatively narrow voltage conversion gain of the module, so this could be a constraint while applying batteries of different voltage. The voltage conversion gain is partly determined in this case by the high-frequency transformer with fixed transformation ratio [89].

The flexibility of PCS #4 is investigated in diverse literature [36] and [40]. In [36] flexibility is addressed by investigating power balancing algorithms among the different modules of the MMCC. Provided that the number of modules in each of the arms of the converter is large –even including reserve modules–, the possibility of applying sorting strategies for the modules while switching is one of the key features of this type of PCSs. Power balancing algorithms permit to balance the state-of-charge among batteries while still having modules in cascade, as for PCSs #2 and #3. The importance of such power balancing algorithms is not only identified as a performance of PCSs based on MMCC but as a necessity, highlighting the challenging control of this type of PCSs. For instance, as reported in [40], even with the same number of modules turned-on, the inclusion of batteries of different voltage at the different modules, may lead to uncontrolled currents flowing through the arms of the converter, thus creating additional losses and harmonics. Power balancing algorithms are of principal importance to turn such circulating currents not as a problem, but as a way to let modules to exchange power between each other yielding a balanced structure [90], [91].

Around the flexibility of PCS #5, remarkable issues are derived from the cascade connection of the different modules interfacing the battery packs with the front-end inverter. By connecting the batteries in cascade, the capacity of the association (in Ah) is limited to the capacity of the weakest battery pack, since the net charging or discharging current provided by the whole association flows through each battery pack. So, to maximize the available energy capacity of the association, power balancing control mechanisms should be included. This aspect is addressed in [53]. The authors proposes a control structure for the modules in cascade in which each one is controlled through two control loops. The inner loop manages the current exchanged by the corresponding battery pack enabling power sharing with the rest of the packs or modules. The control reference for the inner current control loop is determined by an outer (and slower) voltage control loop. This current control loop reference needs to be dynamically varied with respect to battery parameters and, as a result, the bandwidth for the control loops of the different modules can sensibly vary, thus affecting the interoperability of the cascaded association. Among the conclusions of the work, the authors claim that a control system based on conventional proportional-integral controllers in cascade cannot guarantee the stability of the system in all operating conditions. Problems arise specially at the end of charging and discharging cycles, eventually provoking inadvertent tripping in the converter. The problem addressed above is exacerbated

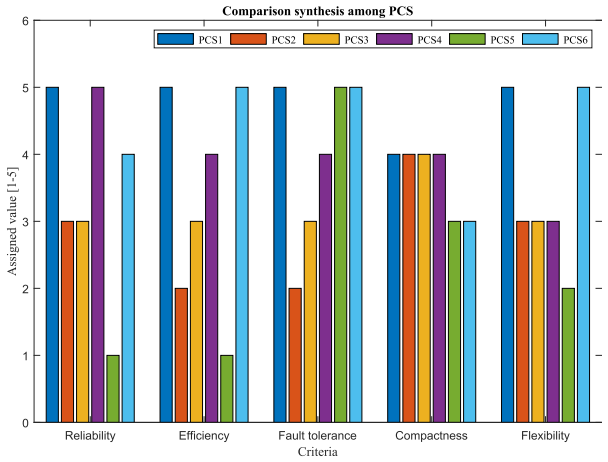

FIGURE 5. Comparison synthesis among PCSs.

while considering the inclusion of battery packs of different characteristics, as considered in [92]. There, the setpoints for the voltage and current control loops for the modules are derived from an optimization problem.

Finally, PCS #6 is identified as a PCS with maximum flexibility, in the level of PCS #1. Here, in each power train, the dc-dc power conversion stage interfacing the battery pack terminals with the dc-link of the front-end inverter controls the charge and discharge profiles of the batteries. Since parallelized, each dc-dc converter of each power train can perform different charge and discharge profiles following the instructions of an energy management system. So no modules in cascade limiting and / or affecting the capabilities of the whole system.

IV. COMPARISON SYNTHESIS

Based on the different exercises comparing PCSs in the previous section III, following contents remark the most important aspects:

- PCS #1 through its different variants, is identified as the most convenient option addressing all criteria considered in this paper. This is reliable, efficient, flexible, compact, as well as it offers good performance under faults.
- PCS #6 follows PCS #1 in most of the criteria considered in this paper. Thus, it is considered also as a good candidate for modular battery based solutions, with the potential of even improve the performance of PCS #1, by using less power converters.
- MMCC structures, as those considered in PCS #2 to #4, are identified as promising options in the future. Research and development should concentrate here in the development of power sharing algorithms that ensure the balance of charge among the different battery packs. This would permit to overcome the drawbacks of connecting in cascade different battery packs.
- Finally, PCS #5 is identified as the weakest configuration among eligible. The connection of different battery packs in cascade, configuring a medium voltage dc-link that is to be managed by a single three-phase front-end inverter, is identified as a hardly reliable option, as well as poorly flexible and efficient one.

Complementing such conclusions, Figure 5 offers a graphical comparison synthesis among PCSs.

V. CONCLUSION

This work developed a comparison among different PCSs for modular battery-based solutions. Six main PCSs, along with their corresponding variants were identified. Variants refer to the number of power conversion steps included in each of the modules composing the PCSs. A first classification of the different PCSs proposed in literature, patents and those actually developed by industry in projects, serve to identify the parallel connection of different and independent power trains to a single point of common coupling with the network, as the most proposed one, specially by industry in projects. This first classification also identified the structures based on MMCC as particularly explored by academia for research and development purposes. The large number of papers addressing such topologies supports this affirmation.

After the above mentioned first classification, this paper proposed a quantitative / qualitative comparison among the different PCSs, also including the different variants at module level. In particular, the discussion addressed various aspects, such as reliability, efficiency, fault tolerance, compactness and operational flexibility. Reliability is assessed through the MTBF metric criteria. To calculate this metric, public database for MIL-HDBK 217 method is adopted. Efficiency metric for each PCS is calculated including conduction and switching losses of transistors, efficiency of batteries and those related to high-frequency transformers. Fault tolerance of PCSs is based on the index Fault Tolerance Index (FTI), metric proposed in the present paper. This metric is based on the quantification of the time derivative of the current when a fault in the grid terminals of the PCS appears. Compactness is evaluated through components counting for each of the PCS. Based on that, along with weighting coefficients for components depending on power density, the volume of each of the PCSs can be evaluated. Finally, the operational flexibility of PCSs is discussed qualitatively. Flexibility refers to the ability to manage the PCS under circumstances such as the connection of batteries of different type and the need of applying state-of-charge balancing methods.

From this work, included in Section III, the authors conclude that PCS #1 (the parallel connection of different power trains to a single point of common coupling), is actually the most reliable, efficient, compact, flexible and with best performance in regard of fault tolerance, among eligible options. The quantitative comparison also serve to identify PCS #6 (the parallel association of dc-dc conversion steps interfacing different battery packs to a single dc-link which in turn is connected to a three-phase inverter), as one promising option for modular battery-based solutions also. It offers excellent

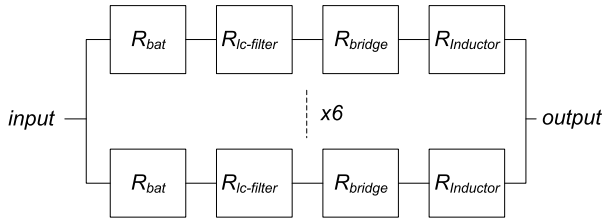

FIGURE 6. Reliability block diagram for PCS #1 and #4, variant (a).

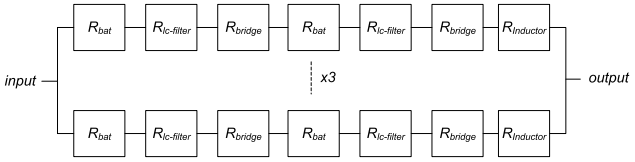

FIGURE 7. Reliability block diagram for PCS #2 and #3, variant (a).

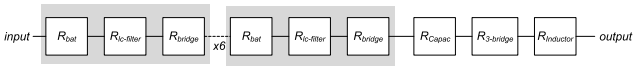

FIGURE 8. Reliability block diagram for PCS #5, variant (a).

performance in regard of efficiency, flexibility and fault tolerance, with the potentiality of configuring a solution with less volume than PCS #1.

Further, the comparison identified MMCC-based PCSs (PCSs #2 to #4) as promising ones in the future, but with the need of overcoming the drawbacks of connecting different modules in cascade. Further even, the problems derived from connecting of modules in cascade are exacerbated in the PCS #5 (the cascaded association of dc-dc conversion steps interfacing different battery packs to a single dc-link which in turn is connected to a three-phase inverter), greatly affecting the reliability and efficiency of this topology.

APPENDIX

RELIABILITY BLOCK DIAGRAMS AND MATHEMATICAL EXPRESSIONS

Figures 6 to 8 present the reliability block diagrams for PCS #1 to #5 (variant a)). For PCS #1 and #4 variant (a), it reads:

$$R_{PCS1a} = R_{PCS4a} = 1 - (1 - R_{bat} \cdot R_{lc} \cdot R_{bridge} \cdot R_l)^6. \quad (29)$$

For PCS #2 and #3 variant (a), it reads:

$$R_{PCS2a} = R_{PCS3a} = 1 - (1 - (R_{bat} \cdot R_{lc} \cdot R_{bridge} \cdot R_l)^2)^3. \quad (30)$$

For PCS #5 variant (a), it reads:

$$R_{PCS5a} = R_{bat} \cdot R_{lc} \cdot R_{bridge} \cdot R_{cap} \cdot R_{3-bridge} \cdot R_l. \quad (31)$$

EFFICIENCY BLOCK DIAGRAMS AND MATHEMATICAL EXPRESSIONS

Figure 9 present the efficiency block diagram for PCS #1 to #4 variant (a). The corresponding mathematical expression is

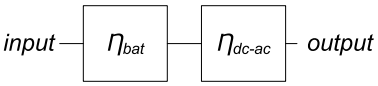

FIGURE 9. Efficiency block diagram for PCS #1 to PCS #4, variant (a).

depicted in the following:

$$\eta_{PCS1a} = \eta_{PCS2a} = \eta_{PCS3a} = \eta_{PCS4a} = \eta_{bat} \cdot \eta_{dc-ac}. \quad (32)$$

REFERENCES

[1] F. Díaz-González, A. Sumper, and O. Gomis-Bellmunt, *Energy Storage in Power Systems*. Hoboken, NJ, USA: Wiley, 2016.

[2] *DOE Global Energy Storage Database*. Accessed: Jan. 5, 2020. [Online]. Available: https://www.energystorageexchange.org/

[3] L. Baruschka and A. Mertens, "Comparison of cascaded H-bridge and modular multilevel converters for BESS application," in *Proc. Energy Convers. Congr. Expo. (ECCE)*, Phoenix, AZ, USA, Sep. 2011, pp. 909–916.

[4] M. Bragard, N. Soltau, S. Thomas, and R. W. De Doncker, "The balance of renewable sources and user demands in grids: Power electronics for modular battery energy storage systems," *IEEE Trans. Power Electron.*, vol. 25, no. 12, pp. 3049–3056, Dec. 2010.

[5] S. Chakraborty, B. Kramer, and B. Kroposki, "A review of power electronics interfaces for distributed energy systems towards achieving low-cost modular design," *Renew. Sustain. Energy Rev.*, vol. 13, no. 9, pp. 2323–2335, Dec. 2009.

[6] T. Soong and P. W. Lehn, "Evaluation of emerging modular multilevel converters for BESS applications," *IEEE Trans. Power Del.*, vol. 29, no. 5, pp. 2086–2094, Oct. 2014.

[7] J. I. Y. Ota, T. Sato, and H. Akagi, "Enhancement of performance, availability, and flexibility of a battery energy storage system based on a modular multilevel cascaded converter (MMCC-SSBC)," *IEEE Trans. Power Electron.*, vol. 31, no. 4, pp. 2791–2799, Apr. 2016.

[8] O. Oghorada and L. Zhang, "Analysis of star and delta connected modular multilevel cascaded converter-based STATCOM for load unbalanced compensation," *Int. J. Electr. Power Energy Syst.*, vol. 95, pp. 341–352, Feb. 2018.

[9] F. Martinez-Rodrigo, S. De Pablo, and L. C. Herrero-de Lucas, "Current control of a modular multilevel converter for HVDC applications," *Renew. Energy*, vol. 83, pp. 318–331, Nov. 2015.

[10] A. P. Mohammad Reza and M. H. Ali, "An optimized SVPWM switching strategy for three-level NPC VSI and a novel switching strategy for three-level two-quadrant chopper to stabilize the voltage of capacitors," *Energy*, vol. 35, no. 12, pp. 4917–4931, Dec. 2010.

[11] S. Wall and D. Mcshane, "A strategy for low-cost utility connection of battery energy storage systems," *J. Power Sources*, vol. 67, nos. 1–2, pp. 193–200, Jul. 1997.

[12] *M5BAT Project Website*. Accessed: Oct. 20, 2019. [Online]. Available: http://m5bat.de/de-de/Projekt

[13] *Siemens Siestorage Product Description*. Accessed: Jan. 20, 2016. [Online]. Available: http://w3.siemens.com/

[14] *Nice Grid EU Project Website*. Accessed: Oct. 21, 2019. [Online]. Available: http://www.nicegrid.fr/

[15] R. Jeanneret, "Apparatus with discrete circuits for charging electrical accumulator with multiple group of cells," U.S. Patent 5 412 305, May 2, 1995.

[16] B. Zhao, Q. Song, W. Liu, and Y. Sun, "Overview of dual-active-bridge isolated bidirectional DC–DC converter for high-frequency-link power-conversion system," *IEEE Trans. Power Electron.*, vol. 29, no. 8, pp. 4091–4106, Aug. 2014.

[17] N. M. L. Tan, T. Abe, and H. Akagi, "Design and performance of a bidirectional isolated DC-DC converter for a battery energy storage system," *IEEE Trans. Power Electron.*, vol. 27, no. 3, pp. 1237–1248, Feb. 2012.

[18] L. Tolbert, F. Zheng Peng, and T. Habetler, "Multilevel converters for large electric drives," *IEEE Trans. Ind. Appl.*, vol. 35, no. 1, pp. 36–44, Jan. 1999.

[19] L. Tolbert, F. Zheng Peng, T. Cunnyngham, and J. Chiasson, "Charge balance control schemes for cascade multilevel converter in hybrid electric vehicles," *IEEE Trans. Ind. Electron.*, vol. 49, no. 5, pp. 1058–1064, Oct. 2002.

[20] L. Maharjan, S. Inoue, H. Akagi, and J. Asakura, "State-of-charge (SOC)-balancing control of a battery energy storage system based on a cascade PWM converter," *IEEE Trans. Power Electron.*, vol. 24, no. 6, pp. 1628–1636, Jun. 2009.
[21] L. Maharjan, S. Inoue, H. Akagi, and J. Asakura, "Fault-tolerant control for a battery energy storage system based on a cascade PWM converter," in *Proc. IEEE 6th Int. Power Electron. Motion Control Conf.*, Wuhan, China, May 2009, pp. 945–950.
[22] L. Maharjan, T. Yamagishi, and H. Akagi, "Active-power control of individual converter cells for a battery energy storage system based on a multilevel cascade PWM converter," *IEEE Trans. Power Electron.*, vol. 27, no. 3, pp. 1099–1107, Mar. 2012.
[23] K. Kandasamy, M. Vilathgamuwa, and K. J. Tseng, "Inter-module state-of-charge balancing and fault-tolerant operation of cascaded H-bridge converter using multi-dimensional modulation for electric vehicle application," *IET Power Electron.*, vol. 8, no. 10, pp. 1912–1919, Oct. 2015.
[24] J. Rodriguez, J.-S. Lai, and F. Zheng Peng, "Multilevel inverters: A survey of topologies, controls, and applications," *IEEE Trans. Ind. Electron.*, vol. 49, no. 4, pp. 724–738, Aug. 2002.
[25] C.-M. Young, N.-Y. Chu, L.-R. Chen, Y.-C. Hsiao, and C.-Z. Li, "A single-phase multilevel inverter with battery balancing," *IEEE Trans. Ind. Electron.*, vol. 60, no. 5, pp. 1972–1978, May 2013.
[26] S. Thomas, M. Stieneker, and R. W. De Doncker, "Development of a modular high-power converter system for battery energy storage systems," in *Proc. 14th Eur. Conf. Power Electron. Appl.*, Birmingham, U.K., 2011, pp. 1–11.
[27] N. Kawakami, S. Ota, H. Kon, S. Konno, H. Akagi, H. Kobayashi, and N. Okada, "Development of a 500-kW modular multilevel cascade converter for battery energy storage systems," *IEEE Trans. Ind. Appl.*, vol. 50, no. 6, pp. 3902–3910, Nov. 2014.
[28] K. Tsang and W. Chan, "27-level DC–AC inverter with single energy source," *Energy Convers. Manage.*, vol. 53, no. 1, pp. 99–107, Jan. 2012.
[29] R. H. Baker and L. H. Bannister, "Electric power converter," U.S. Patent 3867643, Feb. 18, 1975.
[30] N. Mukherjee and D. Strickland, "Modular ESS with second life batteries operating in grid independent mode," in *Proc. 3rd IEEE Int. Symp. Power Electron. Distrib. Gener. Syst.*, Aalborg, Denmark, Jun. 2012, pp. 653–660.
[31] M. Vasiladiotis and A. Rufer, "Balancing control actions for cascaded H-bridge converters with integrated battery energy storage," in *Proc. 15th Eur. Conf. Power Electron. Appl. (EPE)*, Lille, France, Sep. 2013, pp. 1–10.
[32] I. M.-N. S. Trintis and R. Teodorescu, "Cascaded H-bridge with bidirectional boost converters for energy storage," in *Proc. Power Electron. Appl. (EPE)*, Birmingham, U.K., 2011, pp. 1–9.
[33] M. Vasiladiotis and A. Rufer, "A modular multiport power electronic transformer with integrated split battery energy storage for versatile ultrafast EV charging stations," *IEEE Trans. Ind. Electron.*, vol. 62, no. 5, pp. 3213–3222, May 2015.
[34] H. Akagi, "Classification, terminology, and application of the modular multilevel cascade converter (MMCC)," *IEEE Trans. Power Electron.*, vol. 26, no. 11, pp. 3119–3130, Nov. 2011.
[35] M. Hagiwara and H. A. A. Akagi, "Experiment simulation of modular push-pull PWM converter for battery energy storage system," *IEEE Trans. Ind. Appl.*, vol. 50, no. 2, pp. 1131–1140, Jul. 2014.
[36] M. Tsirinomeny and A. Rufer, "Configurable modular multilevel converter (CMMC) for flexible EV," in *Proc. 17th Eur. Conf. Power Electron. Appl.*, Geneva, Switzerland, Sep. 2015, pp. 1–10.
[37] S. L. D'Arco Piegari and P. Tricoli, "A modular converter with embedded battery cell balancing for electric vehicles," in *Proc. Elect. Syst. Aircr., Railway Ship Propuls.*, Bologna, Italy, Oct. 2012, pp. 1–6.
[38] F. Gao, L. Zhang, and Q. Zhou, "State-of-charge balancing control strategy of battery energy storage system based on modular multilevel converter," in *Proc. IEEE Energy Convers. Congr. Expo. (ECCE)*, Pittsburgh, PA, USA, Sep. 2014, pp. 2567–2574.
[39] N. Li, F. Gao, T. Hao, Z. Ma, and C. Zhang, "SOH balancing control method for the MMC battery energy storage system," *IEEE Trans. Ind. Electron.*, vol. 65, no. 8, pp. 6581–6591, Aug. 2018.
[40] M. Quraan, T. Yeo, and P. Tricoli, "Design and control of modular multilevel converters for battery electric vehicles," *IEEE Trans. Power Electron.*, vol. 31, no. 1, pp. 507–517, Jan. 2016.
[41] E. Prieto-Araujo, A. Junyent-FerrÉ, C. Collados-Rodríguez, G. Clariana-Colet, and O. Gomis-Bellmunt, "Control design of Modular Multilevel Converters in normal and AC fault conditions for HVDC grids," *Electr. Power Syst. Res.*, vol. 152, pp. 424–437, Nov. 2017.
[42] G. Demetriades, "Modular multilevel converter with cell-connected battery storages," U.S. Patent 8 760 122 B2, Jun. 24, 2014.
[43] R. Bin, X. Yonghai, and L. Qiaoqian, "A control method for battery energy storage system based on MMC," in *Proc. IEEE 2nd Int. Future Energy Electron. Conf. (IFEEC)*, Taipei, Taiwan, Nov. 2015, pp. 1–6.
[44] Z. Wang, H. Lin, and Y. Ma, "Improved capacitor voltage balancing control for multimode operation of modular multilevel converter with integrated battery energy storage system," *IET Power Electron.*, vol. 12, no. 11, pp. 2751–2760, 2019, doi: 10.1049/iet-pel.2019.0033.
[45] P. Guo, Q. Xu, Y. Yue, F. Ma, Z. He, A. Luo, and J. Guerrero, "Analysis control of modular multilevel converter with split energy storage for railway traction power conditioner," *IEEE Trans. Power Electron.*, to be published, doi: 10.1109/TPEL.2019.2917065.
[46] A. Hillers and J. Biela, "Optimal design of the modular multilevel converter for an energy storage system based on split batteries," in *Proc. 15th Eur. Conf. Power Electron. Appl. (EPE)*, Lille, France, Sep. 2013, pp. 1–11.
[47] A. Hillers and J. Biela, "Fault-tolerant operation of the modular multilevel converter in an energy storage system based on split batteries," in *Proc. 16th Eur. Conf. Power Electron. Appl.*, Lappeenranta, Finland, Aug. 2014, pp. 1–8.
[48] D. Montesinos-Miracle, M. Massot-Campos, J. Bergas-Jane, S. Galceran-Arellano, and A. Rufer, "Design and control of a modular multilevel DC/DC converter for regenerative applications," *IEEE Trans. Power Electron.*, vol. 28, no. 8, pp. 3970–3979, Aug. 2013.
[49] Y. Li and Y. Han, "A module-integrated distributed battery energy storage and management system," *IEEE Trans. Power Electron.*, vol. 31, no. 12, pp. 8260–8270, Jan. 2016.
[50] S. Bhowmik and E. Macris, "Systems and methods for scalable configurations of intelligent energy storage packs," U.S. Patent 2010/0 305 770 A1, Apr. 1, 2010.
[51] J. A. Qahouq, "Distributed battery power electronics architecture and control," U.S. Patent 2014/0 125 284 A1, Jun. 14, 2016.
[52] N. Mukherjee and D. Strickland, "Control of second-life hybrid battery energy storage system based on modular boost-multilevel buck converter," *IEEE Trans. Ind. Electron.*, vol. 62, no. 2, pp. 1034–1046, Jul. 2015.
[53] N. Mukherjee and D. Strickland, "Control of cascaded DC-DC converter-based hybrid battery energy storage systems—Part I: Stability issue," *IEEE Trans. Ind. Electron.*, vol. 63, no. 4, pp. 2340–2349, Jul. 2016.
[54] N. Mukherjee and D. Strickland, "Control of cascaded DC–DC converter-based hybrid battery energy storage Systems—Part II: Lyapunov approach," *IEEE Trans. Ind. Electron.*, vol. 63, no. 5, pp. 3050–3059, May 2016.
[55] V. Kanakasabai and B. Sen, "Modular stacked dc architecture traction system and method of making same," U.S. Patent 2013/0 134 911 A1, Jan. 6, 2015.
[56] J. U. Lim, S. J. Lee, and K. P. Kang, "A modular power conversion system for zinc-bromine flow battery based energy storage system," in *Proc. IEEE 2nd Int. Future Energy Electron. Conf. (IFEEC)*, Taipei, Taiwan, Nov. 2015, pp. 1–5.
[57] S. Rothgang, T. Baumhöfer, H. Van Hoek, T. Lange, R. W. De Doncker, and D. U. Sauer, "Modular battery design for reliable, flexible and multi-technology energy storage systems," *Appl. Energy*, vol. 137, pp. 931–937, Jan. 2015.
[58] F. Caponio, A. Abba, and P. Baruzzi, "Modular and bi-directional energy storage system compliant with accumulators of different chemistry," in *Proc. Elect. Power Qual. Utilisation (EPQU)*, Lisbon, Portugal, Oct. 2011, pp. 1–6.
[59] B. Xie, Y. Liu, Y. Ji, and J. Wang, "Two-stage battery energy storage system (BESS) in AC microgrids with balanced state-of-charge and guaranteed small-signal stability," *Energies*, vol. 11, no. 2, p. 322, Feb. 2018.
[60] K. Sayed and H. Gabbar, "Electric vehicle to power grid integration using three-phase three-level AC/DC converter and pi-fuzzy controller," *Energies*, vol. 9, no. 7, p. 532, Jul. 2016.
[61] Z. Zhang, Y.-Y. Cai, Y. Zhang, D.-J. Gu, and Y.-F. Liu, "A distributed architecture based on microbank modules with self-reconfiguration control to improve the energy efficiency in the battery energy storage system," *IEEE Trans. Power Electron.*, vol. 31, no. 1, pp. 304–317, Jan. 2016.
[62] E. C. Fontana and P. Smith, "System and method for combining the outputs of multiple, disparate types of power sources," U.S. Patent 12 831 478, Apr. 1, 2010.
[63] K. Kubo, T. Nomura, N. Tokunaga, H. Miyazaki, and A. Emori, "Charge and discharge system for electric power storage equipment," U.S. Patent 6 297 616 B1, Oct. 2, 2001.

[64] M. Shousha, A. Prodic, V. Marten, and J. Milios, "Design and implementation of assisting converter-based integrated battery management system for electromobility applications," *IEEE J. Emerg. Sel. Topics Power Electron.*, vol. 6, no. 2, pp. 825–842, Jun. 2018.
[65] M. Uno and K. Tanaka, "Influence of high-frequency charge–discharge cycling induced by cell voltage equalizers on the life performance of lithium-ion cells," *IEEE Trans. Veh. Technol.*, vol. 60, no. 4, pp. 1505–1515, May 2011.
[66] *Mitsubishi Power Electronics Website*. Accessed: Feb. 14, 2018. [Online]. Available: http://www.pwrx.com/
[67] D. W. Hart, *Power Electronics*. New York, NY, USA: McGraw-Hill, 2011.
[68] A. Ferreira, "Modular multilevel converters for power system applications," Ph.D. dissertation, Dept. Elect. Eng., Univ. Politècnica de Catalunya, Barcelona, Spain, 2017.
[69] G. Adam, O. Anaya-Lara, G. Burt, D. Telford, B. Williams, and J. Mcdonald, "Modular multilevel inverter: Pulse width modulation and capacitor balancing technique," *IET Power Electron.*, vol. 3, no. 5, pp. 702–715, 2010.
[70] *IEEE Standard Computer Dictionary: A Compilation of IEEE Standard Computer Glossaries*, IEEE Standard 610-1990, 1990.
[71] *MIL-HDBK-217F(N2) Parts Count Prediction Calculator*. Accessed: Apr. 9, 2018. [Online]. Available: http://reliabilityanalyticstoolkit.appspot.com/mil_hdbk_217F_parts_count
[72] M. Čepin, *Assessment of Power System Reliability*. London, U.K.: Springer-Verlag, 2011.
[73] A. Wintrich, U. Nicolai, and W. Tursky, *Application Manual Power Semiconductors* (Semikron International GmbH). Ilmenau, Germany: ISLE Verlag, 2011.
[74] C. Steinmetz, "On the law of hysteresis," *Proc. IEEE*, vol. 72, no. 2, pp. 197–221, Feb. 1984.
[75] E. Kontos, G. Tsolaridis, R. Teodorescu, and P. Bauer, "On DC fault dynamics of MMC-based HVdc connections," *IEEE Trans. Power Del.*, vol. 33, no. 1, pp. 497–507, Feb. 2018.
[76] B. Li, J. He, and J. Tian, "DC fault analysis for modular multilevel converter-based system," *J. Mod. Power Syst. Clean Energy*, vol. 5, no. 2, pp. 275–282, 2017.
[77] J. Yang, J. E. Fletcher, and J. O'Reilly, "Short-circuit and ground fault analyses and location in VSC-based DC network cables," *IEEE Trans. Ind. Electron.*, vol. 59, no. 10, pp. 3827–3837, Oct. 2012.
[78] X. N. Zhang, C. Y. Zhao, and H. Pang, "A control and protection scheme of multi-terminal DC transmission system based on MMC for DC line fault," *Autom. Electr. Power Syst.*, vol. 37, no. 15, pp. 140–145, 2013.
[79] B. Mitra and B. Chowdhury, "Comparative analysis of hybrid DC breaker and assembly HVDC breaker," *North Amer. Power Symp. (NAPS), Morgantown, Sep. 2017*, pp. 1–6.
[80] L. Tang and B.-T. Ooi, "Locating and isolating DC faults in multi-terminal DC systems," *IEEE Trans. Power Del.*, vol. 22, no. 3, pp. 1877–1884, Jul. 2007.
[81] F. Chang, Z. Yang, and Y. Wang, "Fault characteristics and control strategies of multiterminal high voltage direct current transmission based on modular multilevel converter," *Math. Problems Eng.*, vol. 2015, p. 11, 2015, Art. no. 502372, doi: 10.1155/2015/502372.
[82] G. Li, J. Liang, and F. Ma, "Analysis of single-phase-to-ground faults at the valve-side of HB-MMCs in bipolar HVDC systems," in *Proc. IEEE Energy Convers. Congr. Expo. (ECCE)*, Cincinnati, OH, USA, Oct. 2017, pp. 1–6.
[83] *General Electric. Dry Type Transformers for General Purpose, Aluminum, Three-Phase DOE 2016 Efficiency*. Accessed: Dec. 12, 2017. [Online]. Available: http://www.geindustrial.com/buylog_pdf
[84] *REO-USA, HPTA/603 Transformer*. Accessed: Dec. 12, 2017. [Online]. Available: http://www.reo-usa.com/
[85] *Chint Power Systems 30 kW Storage Inverter for North America*. Accessed: Dec. 12, 2017. [Online]. Available: https://www.chintpowersystems.com/
[86] D. Bazargan, S. Filizadeh, and A. M. Gole, "Stability analysis of converter-connected battery energy storage systems in the grid," *IEEE Trans. Sustain. Energy*, vol. 5, no. 4, pp. 1204–1212, Oct. 2014.
[87] Z. Liu, C. Tan, and F. Leng, "A reliability-based design concept for lithium-ion battery pack in electric vehicles," *Rel. Eng. Syst. Saf.*, vol. 134, pp. 169–177, Jan. 2015.
[88] M. Manjrekar, P. Steimer, and T. Lipo, "Hybrid multilevel power conversion system: A competitive solution for high-power applications," *IEEE Trans. Ind. Appl.*, vol. 36, no. 3, pp. 834–841, May 2000.
[89] D. Sha, G. Xu, and Y. Xu, "Utility direct interfaced charger/discharger employing unified voltage balance control for cascaded H-bridge units and decentralized control for CF-DAB modules," *IEEE Trans. Ind. Electron.*, vol. 64, no. 10, pp. 7831–7842, Jun. 2017.
[90] Y. Zhang, Q. Ge, and R. Zhang, "The control of arm currents and the parameters for modular multilevel converters," in *Proc. 15th Int. Conf. Elect. Mach. Syst.*, Sapporo, Japan, 2012, pp. 1–6.
[91] Z. Alaas, C. Wang, C. Jiang, C. Duan, and L. Y. Wang, "A hierarchal cascaded multilevel converter for uniform SOC battery management," in *Proc. IEEE Transp. Electrific. Conf. Expo (ITEC)*, Dearborn, MI, USA, Jun. 2016, pp. 1–6.
[92] N. Mukherjee, D. Strickland, and M. A. Varnosfaderani, "Adaptive control of hybrid battery energy storage systems under capacity fade," in *Proc. 16th Eur. Conf. Power Electron. Appl. (EPE-ECCE Eur.)*, Lappeenranta, Finland, 2014, pp. 1–10.

FRANCISCO DÍAZ-GONZÁLEZ was born in Barcelona, Spain, in 1983. He received the degree in industrial engineering from the School of Industrial Engineering of Barcelona, Universitat Politècnica de Catalunya (UPC), Barcelona, Spain, in 2009, and the Ph.D. degree in electrical engineering from UPC, in 2013. Since 2016, he has been with UPC. He is currently working as a Lecturer (Serra Húnter programme) and a Researcher with UPC on projects related to energy storage technologies and renewable-based generating systems. His research activity is in the Centre d'Innovació Tecnològica en Convertidors Estàtics i Accionaments (CITCEA-UPC). He has authored one book on energy storage for power systems, published more than 20 articles in peer-reviewed journals and international conferences, and holds one patent.

DANIEL HEREDERO-PERIS was born in Vilanova i la Geltrú, Spain, in 1985. He received the M.Sc. degree in control engineering and the Ph.D. degree from the School of Industrial Engineering of Barcelona, Universitat Politècnica de Catalunya (UPC), in 2010 and 2017, respectively. Since 2010, he has been working with the Centre d'Innovació Tecnològica en Convertidors Estàtics i Accionaments (CITCEA-UPC) as a Project Engineer developing tasks focused in design of algorithms related to the control of grid-connected and standalone single/three-phase inverters, and V2G projects for EV. His main research interests are control of power electronics, micro-grids, and EVs.

MARC PAGÈS-GIMÉNEZ was born in Barcelona, Spain, in 1982. He received the M.Sc. degree in electrical engineering from the School of Industrial Engineering of Barcelona (ETSEIB), Universitat Politècnica de Catalunya (UPC), Barcelona, Spain, in 2009. From 2009 to 2017, he was involved with the Centre d'Innovació Tecnològica en Convertidors Estàtics i Accionaments (CITCEA-UPC) as a Project Engineer, where he mainly carried out the development of hardware and software concerning power converters for grid integration of distributed generation and storage devices. Since 2018, he has been the CTO in Tekno-CEA, a spin-off of CITCEA-UPC.

EDUARDO PRIETO-ARAUJO (Member, IEEE) was born in Premià de Mar, Spain, in 1986. He received the degree in industrial engineering from the School of Industrial Engineering of Barcelona (ETSEIB), Universitat Politècnica de Catalunya (UPC), Barcelona, Spain, in 2011, and the Ph.D. degree in electrical engineering from UPC, in 2016. Since 2010, he has been with CITCEA-UPC Research Group. He is currently a Lecturer with the Electrical Engineering Department, UPC. He is also participating in CIGRE Working groups B4.70 and B4.81 and Task Force B4.77, both related with HVDC converters. He is also a Lecturer of the Serra Húnter programme. His main interests are renewable generation systems, control of power converters for HVDC applications, and interaction analysis between converters and power electronics dominated power systems.

ANDREAS SUMPER (Member, IEEE) was born in Villach, Austria. He received the Dipl.Ing. degree in electrical engineering from the Technical University of Graz, Styria, Austria, in 2000, and the Ph.D. degree from the Universitat Politècnica de Catalunya, Barcelona, Spain, in 2008. From 2001 to 2002, he was a Project Manager for innovation projects in private industry. In 2002, he joined the Centre d'Innovació Tecnològica en Convertidors Estàtics i Accionaments (CITCEA-UPC). Since 2019, he is a Full Professor with the Department of Electrical Engineering, School of Industrial Engineering of Barcelona (ETSEIB), Universitat Politècnica de Catalunya, Barcelona.